Experimental observations and matching viscoelastic specific work predictions of flow-induced crystallization for molten polyethylene within two flow geometries

L. Scelsi and M. R. MackleyH. Klein and P. D. OlmstedR. S. GrahamO. G. HarlenT. C. B. McLeish

Citation: Journal of Rheology **53**, 859 (2009); doi: 10.1122/1.3123209
View online: http://dx.doi.org/10.1122/1.3123209
View Table of Contents: http://sor.scitation.org/toc/jor/53/4
Published by the The Society of Rheology

Experimental observations and matching viscoelastic specific work predictions of flow-induced crystallization for molten polyethylene within two flow geometries

L. Scelsi and M. R. Mackley[a)]

Department of Chemical Engineering and Biotechnology, University of Cambridge, Pembroke Street, Cambridge, CB2 3RA, United Kingdom

H. Klein and P. D. Olmsted

Polymer IRC, School of Physics and Astronomy, University of Leeds, Leeds LS2 9JT, United Kingdom

R. S. Graham

School of Mathematical Sciences, University of Nottingham, Nottingham NG7 2RD, United Kingdom

O. G. Harlen

Department of Applied Mathematics, University of Leeds, Woodhouse Lane, Leeds, LS2 9JT, United Kingdom

T. C. B. McLeish

Departments of Physics and Chemistry, Durham University, Durham, DH1 3HP, United Kingdom

(Received 13 November 2008; final revision received 2 April 2009)

Synopsis

Flow-induced crystallization (FIC) behavior of a high-density polyethylene melt in two entry-exit flow geometries was investigated by direct optical observation using a multi-pass rheometer and the results compared with a viscoelastic flow simulation. A set of experiments was performed at several piston speeds using a sharp and a rounded entry-exit slit and the region of onset for visible FIC was identified in both cases. During flow narrow crystal filament regions localized at the sidewalls and in a downstream "fang" region of stress accumulation were identified. A melt flow two-dimensional numerical simulation using a Lagrangian solver, FLOWSOLVE, and an 11-mode Pom-Pom model satisfactorily matched experimental pressure difference and birefringence fringe distribution for the flow. An algorithm to calculate the specific work accumulated by each fluid element in the complex flow field was implemented within FLOWSOLVE and a method was proposed

[a)]Author to whom correspondence should be addressed; electronic mail: mrm5@cheng.cam.ac.uk

to estimate the critical specific work for the onset of visible oriented FIC. The concept of specific work applied to the numerical simulations was capable of successfully predicting the experimental regions where FIC occurred. © *2009 The Society of Rheology.* [DOI: 10.1122/1.3123209]

I. INTRODUCTION

The development of flow-induced crystallization (FIC) during a forming process can determine the microstructure and, subsequently, the end properties of semi-crystalline polymer products. Flow in general can either enhance spherulitic isotropic crystallization [see, for example, Eder *et al.* (1990) and Jay *et al.* (1999)] or induce fibrous nuclei that then form shish-kebab like fibrous crystals [see, for example, Keller (1968) and Mackley *et al.* (2000)] and in industrial processes different types of FIC can occur simultaneously under complex thermo-mechanical histories. In the case of injection molding, for instance, both the complex flow and the presence of temperature gradients are responsible for the onset of different crystal morphologies, which are a function of the local thermo-mechanical history. Generally, a transcrystalline layer [Billon *et al.* (2002)], an oriented skin layer of shish kebabs, and a spherulitic core can coexist in the same sample [Jerschow and Janeschitz-Kriegl (1996)].

Significant interest in FIC of polymer melts has been shown in recent years and insight has been gained on the mechanism of oriented shish-kebab structure formation. Several research groups worldwide performed rheo-optical and combined small and wide angle x-ray scattering studies on bimodal blends of a low molecular weight crystallizable polymer matrix and a small fraction of high molecular weight polymer using a standardized "short term shearing" protocol [Liedauer *et al.* (1993)]. The essential role of the high molecular weight fraction in shish formation already proposed by Mackley and Keller (1973) was confirmed [see, for example, Kumaraswamy *et al.* (2000; 2002)]. It is now generally believed that the formation of shish kebabs in sheared melts depends on the existence of meta-stable oriented precursors—that may have undetectable crystallinity—whose formation occurs during flow and is governed by the interplay between crystallization rate and the relaxation time of the long molecules in the melt [see, for instance, Seki *et al.* (2002) and Balzano *et al.* (2008)]. The drastic enhancement in shish-kebab formation for blends in which the concentration of high molecular weight polymer exceeds the chain overlap concentration suggests a cooperative mechanism of shish formation, involving simultaneously several molecules [Seki *et al.* (2002); Somani *et al.* (2005); Heeley *et al.* (2006); Kumaraswamy *et al.* (2004); Matsuba *et al.* (2007)]. The shish-kebab network formed at early times subsequently acts as a template for further crystallization [Somani *et al.* (2005)]. Keum *et al.* (2008) followed the time dependent growth of shishes and kebabs, separately, through careful control of the crystallization temperature and confirmed that the shishes, which formed above the melting temperature, were mainly constituted by extended high-molecular-weight chains, whereas the kebabs, formed at lower temperature, were constituted by coiled chains.

However, a molecularly based model based on these findings that can be applied to polydisperse polymer melts in industrial flows has not yet been proposed at the present day. Modeling of FIC in processing flows is currently limited in most cases to using the modified Avrami modeling of nucleation and growth [Avrami (1939)] as a frame of reference [see, for example, Doufas *et al.* (1999), Smirnova *et al.* (2005), and Zuidema *et al.* (2001)].

The deformation history experienced by the polymer molecules is the result of a combination of shear rate and shear time and is known to influence the crystallization development. One quantity that can be used to describe the deformation history is the

mechanical work done on the sample to generate the flow. The concept of specific work (SW) (represented as work per unit volume) to analyze the effect of flow on FIC of polymer melts was first introduced by Janeschitz-Kriegl and co-workers [see, for example, Janeschitz-Kriegl *et al.* (2003)]. The authors performed experiments on a mildly super-cooled polypropylene and found the nucleation density of enhanced spherulitic crystallization to be proportional to the work undergone by the polymer fluid. A further study by Mykhaylyk *et al.* (2008) on sheared bimodal blends found a correlation between the onset of oriented shish kebab crystallization and the amount of SW undergone by the polymer. For a fixed temperature and blend composition, when shearing above a minimum shear rate necessary to sufficiently extend the chains, the value of the critical SW for the onset of shish kebabs was found to be independent of the value of the shear rate applied during the pulse shear experiments. Although the correlation between SW accumulated by the polymer fluid and FIC has an essentially empirical origin, the physical interpretation given by Mykhaylyk *et al.* (2008) considers the probability of creation of stretched chain segments and the probability of these segments to meet and nucleate a fibrous crystal. The probability of stretch is proportional to the local stress, whereas the probability of meeting is proportional to the strain. The total work that can be written as $w = \int \sigma \, d\gamma$ can then directly be related to the probability of onset of an oriented crystal structure. These results were confirmed by Housmans (2008) and Van Puyvelde *et al.* (2008), who found that the transition between a spherulitic and an oriented morphology for sheared melts, respectively, PP and poly-1-butene, occurred within a narrow range of SW values. These values were independent of the shear rate and decreased with molecular weight.

Extensive work on FIC under complex processing flows has been carried out by several groups [see, for example, McHugh *et al.* (1991) and Peters (2003)] and a multipass rheometer (MPR) has been used at Cambridge in recent years by a number of authors to perform optical and x-ray studies of FIC [see Mackley *et al.* (2000), Hernandez de Muller (2008), Hassell and Mackley (2008), and Scelsi and Mackley (2008)]. During all these complex flow experiments, preferential development of oriented FIC was observed in local regions of the flow.

Recently, the ability to simulate viscoelastic flow of polymer melts in complex flows has improved significantly, as a result of more powerful computational techniques and improved numerical methods [Baaijens (1998)], together with the development of new constitutive models derived from molecular behavior such as the Pom-Pom model [McLeish and Larson (1998)].

This paper demonstrates that the correlation between SW and FIC can be extended to "processing-like" transient flows. A numerical strategy for following the onset of FIC in localized regions of a complex MPR flow has been implemented. This strategy first involved numerically predicting and experimentally validating a viscoelastic complex flow stress field and from this then computing maps of SW within the flow. The SW predictions were subsequently compared with experimental observations of localized FIC. It has been shown that the concept of SW gives consistent predictions with experimental observations and can successfully be applied to predict the onset of localized FIC in the complex flows that were considered.

II. MATERIALS AND METHODS

A. Material

The material used was a metallocene-catalyzed high-density polyethylene (DOW HDB6) with a Mw of 68 000 g/mol and Mw/Mn of 2.08. The polymer belongs to a

TABLE I. Pom-Pom parameters for DOW HDB6 at 125 °C. Parameters obtained by fitting a linear frequency sweep and non-linear extension tests at 155 °C and shift of the data to 125 °C using time-temperature superposition. All data provided by Dr. D. Auhl, University of Leeds.

Mode	1	2	3	4	5	6	7	8	9	10	11
$\tau_{b,i}$ (s^{-1})	0.0078	0.0246	0.078	0.246	0.778	2.461	7.783	24.61	77.83	246.1	778.3
$\tau_{r,i}$ (s^{-1})	0.0078	0.0246	0.078	0.246	0.778	2.461	7.783	24.61	38.92	82.04	389.2
$q_{\text{arms},i}$	1	1	1	1	1	1	1	1	2	5	9
G_i (Pa)	318631	102308	39120	29668	17251	11165	5942	2735	985.2	250.5	52.22

family of high-density polyethylene (HDPE) materials having controlled levels of long-chain branching [for more information, see Woods-Adams and Costeux (2001)]. Non-isothermal differential scanning calorimetry at 10 °C/min identified the following quiescent crystallization temperatures: crystallization onset ~123 °C, peak ~120 °C and end ~113 °C, and a peak melting temperature of ~142 °C. A quasi-static crystallization test in an Advanced Rheometrics Expansion System (ARES) rheometer at 1% strain and 10 rad/s and 125 °C gave an onset crystallization time of the order of 30 min, which therefore gave a processing window to explore FIC without the complication of normal spherulitic crystallization occurring at the same time.

Hassell and Mackley (2008) demonstrated the suitability of DOW HDB6 for MPR FIC experiments in an MPR. DOW HDB6 at 125 °C can crystallize during flow forming crystal filaments that are narrow and well defined.

Linear viscoelasticity and non-linear shear data were obtained using an ARES strain controlled rheometer with parallel plates. Non-linear extension data were obtained using a Sentmanat extensional rheometer fixture. The experimental data at 155 °C were shifted to 125 °C using the time-temperature superposition and were fitted with an 11-mode Pom-Pom model. The model parameters are summarized in Table I.

B. Processing experiments in a MPR

Controlled isothermal complex-flow experiments that resemble elements of polymer processing conditions were carried out using a MPR using its optical configuration. This technique has been previously described by several authors [see, for example, Collis and Mackley (2005)]. The MPR is a dual piston capillary-type rheometer designed for small quantities of material (~12 g of polymer) and consists of three sections. The top and bottom sections contain reservoirs for the polymer material, servo hydraulically driven pistons, and pressure/temperature transducers. The midsection enables simultaneous pressure and optical measurements to be made and resembles a cube with holes through all six faces. The vertical faces accept a pair of stainless steel die inserts in one direction, and a pair of stress-free quartz windows in the other, while polymer flows through the top and bottom holes. All three sections are surrounded by heating channels and insulation. During experiments, the pistons are moved synchronously, forcing the material to flow within the contraction geometry in the midsection. Optical observation was carried out in bright field or through crossed polarizers, using monochromatic polarized light with a wavelength of 514 nm and a digital video camera. The optical train for the flow-induced birefringence (FIB) observations—polarizer lens at 0° to the vertical direction, quarter wave plate at 45°, sample between quartz windows, quarter wave plate at 135°, analyzer lens at 90°—was removed for the bright-field visualization of localized crystallization.

Two different entry-exit geometries were used and their configuration and dimensions are shown in Fig. 1. The first (named CE-1) was a contraction-expansion slit geometry

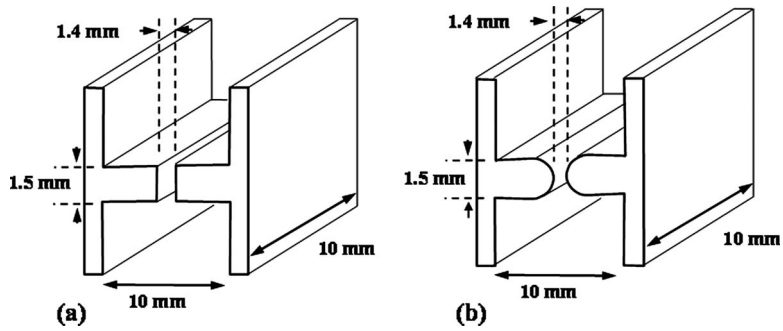

FIG. 1. Schematics and dimensions of the entry exit optical flow cells (a) sharp cornered entry-exit slit (CE-1); (b) rounded entry-exit slit (CE-3).

with sharp corners similar to those used in previous work [see, for instance, Hassell and Mackley (2008)]. The second geometry (CE-3) has similar dimensions to the first one but has completely rounded corners. Within the slit, the aspect ratio of the slits is 10 mm/1.4 mm and this gives a reasonable approximation to two-dimensional (2D). In upstream and downstream of the slit, the aspect ratio is 10 mm/10 mm. The apparent wall shear rate used to estimate the shear rates was based on the solution for Newtonian flow through infinite parallel plates and is given by

$$\dot{\gamma}_{\mathrm{app},w} = \frac{6Q}{w^2 l} = \frac{3\pi D_P^2 V_p}{2w^2 l}, \tag{1}$$

where Q is the volumetric flow rate ($\mathrm{mm^3\ s^{-1}}$), D_p is the piston diameter (10 mm), w is the width of the slit in its narrowest section (1.4 mm), l is the depth of the slit (10 mm), and V_p is the speed of the pistons ($\mathrm{mm\ s^{-1}}$). Both geometries create regions of high simple shear near to the slit walls and extensional flow in the region of the symmetry line in the inlet and outlet areas of the flow. However, under the conditions investigated, FIC occurred near the slit walls only, due to shear.

C. Viscoelastic numerical simulations

All the simulations were performed using the numerical code FLOWSOLVE and were constrained to be two-dimensional and isothermal. FLOWSOLVE is a Lagrangian solver developed at the University of Leeds [Harlen *et al.* (1995); Nicholson (2000)]. The Lagrangian implementation uses a triangular mesh that is changed with every step of the simulation. An example of a satisfactory application of FLOWSOLVE to match entry-exit MPR flows was reported in Collis and Mackley (2005). The constitutive equation used in this study was the Pom-Pom model, which is based on tube theory for a branched molecular geometry having two q-armed stars connected by a backbone segment, with different characteristic relaxation times for the stretch (τ_s) and orientation (τ_b) of the backbone. The multi-mode form of the model has been adopted, with a spectrum of 11 relaxation times. A detailed description of the Pom-Pom equations can be found in the original paper of McLeish and Larson (1998).

The initial mesh and the deformed mesh after 2 s of simulation time for CE-3 geometry and a piston speed of 1 mm/s are shown in Fig. 2. The mesh has three concentric regions of refinement. At the initial stage only the boundaries are specified, as the program fills the area with a regular distribution of vertices at a given density. The stresses across this grid are then calculated from the constitutive parameters and boundary con-

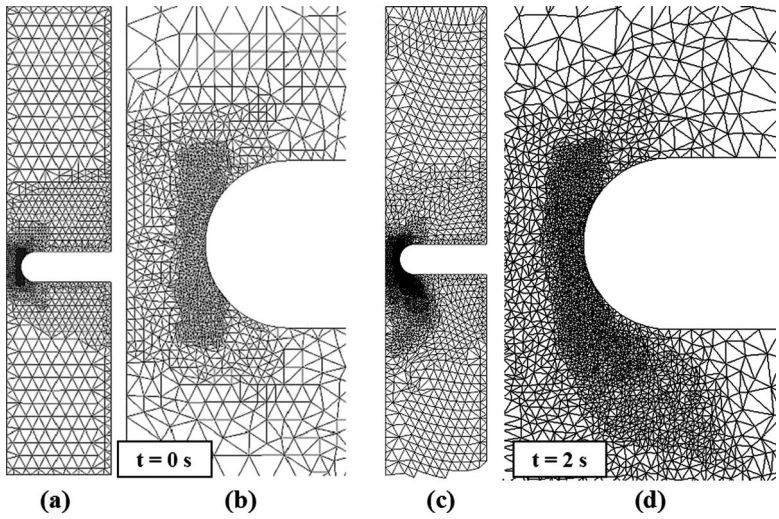

FIG. 2. Mesh for the CE-3 geometry. Mesh at $t=0$. (a) Full view and (b) zoom around the rounded sidewall. The Lagrangian implementation causes remeshing after each time step, leading to substantial modification of the original mesh. Grid after $t=2$ s of simulation time for DOW HDB6 flowing at a piston speed of 1 mm/s. (c) Full view and (d) detail.

ditions and a solution found for the velocities and pressures at each vertex. The triangular elements deform according to these velocities and the constitutive parameters updated to reflect the deformations. The grid is checked to split triangular elements that have become too large, delete those which have become too small, and add new elements at inflow boundaries, before moving to the next step. An algorithm to calculate the SW done on the fluid was implemented in the code. The SW "w" $[\mathrm{J/m^3}]$ accumulated during simple shear flow is given by

$$w = \int_0^t \sigma_{xy}\dot{\gamma}(t')dt', \tag{2}$$

where σ_{xy} and $\dot{\gamma}$ are, respectively, the shear stress and the shear rate and the integration is between time of flow inception and the current time. Generalizing for a complex 2D or three-dimensional flow leads to the following expression for the work experienced by each fluid element during flow:

$$\frac{\partial w}{\partial t} + u \cdot \nabla w \equiv \frac{Dw}{Dt} = \boldsymbol{\sigma}:\nabla \mathbf{u} = \sum_i \sum_j \sigma_{ij}\frac{\partial u_j}{\partial x_i}, \tag{3}$$

involving the components of the stress and the strain rate tensors (σ_{ij} and $\partial u_j/\partial x_i$). At each time, the code computes the SW distribution with respect to the spatial coordinates (x,y) for the entire flow geometry.

The total stress and the stress contribution due to the polymer using a multimode Pom-Pom constitutive equation are, respectively, given by

$$\boldsymbol{\sigma} = -p\mathbf{I} + 2\mu\mathbf{E} + \boldsymbol{\sigma}_\mathbf{P}, \tag{4}$$

(p: pressure, $\mathbf{E}$: deformation tensor, μ: viscosity, and $\sigma_\mathbf{P}$: polymer stress) and

$$\boldsymbol{\sigma}_{\mathbf{P}} = \sum_{i=1}^{m} \lambda_i^2 \cdot G_i(\mathbf{A}_i - \mathbf{I}/3), \tag{5}$$

where λ_i represents the backbone stretch for each mode, m is the number of modes, G_i is the relaxation modulus for each mode, and $\mathbf{A}$ is related to the orientation tensor $\mathbf{S}(t)$. For the full set of Pom-Pom equations implemented in FLOWSOLVE, please refer to Collis and Mackley (2005).

Experimental evidence [Mykhaylyk *et al.* (2008)] suggests that SW counting toward the onset of FIC accumulates only if a minimum shear rate is exceeded in such a way that the molecules involved in the nucleation process are stretched.

This corresponds to the condition

$$\sqrt{2 \cdot \sum_i \sum_j E_{ij} E_{ij}} > \frac{1}{\tau_x}, \tag{6}$$

with $\tau_x \sim \tau_R$ of the largest molecules in the melt.

Finally, the SW can relax with a certain time scale. The proposed work relaxation equation takes the following form:

$$\frac{1}{\tau_w^*} = \begin{cases} \dfrac{1}{\tau_w}(1 - w/w_e) & \text{if} \quad w < w_c \\ 0 & \text{if} \quad w \geq w_c. \end{cases} \tag{7}$$

As the SW accumulates, its relaxation time (τ_w^*) increases and finally reaches infinity when the SW exceeds a critical value (w_c). In relation to the set of FIC experiments presented, a systematic set of simulations involving a variation of the work parameters within a wide range ($\tau_x = 10^{-1} - 10^3$; $\tau_w = 10^{-1} - 10^4$; and $w_c = 1 - 10^5$) has proved that, for a piston speed of 1 mm/s, the calculated SW is almost completely insensitive to the value of τ_x, τ_w, and w_c. This can be explained by the fact that, in all cases, the stretch condition (6) is satisfied for most of the observation region and at the same time the work relaxation mechanism does not come into play due to the short time scale of the crystallization experiment with respect to τ_w. The values for τ_x, τ_w, and w_c were chosen to be 389 s, 778 s, and 1 MPa, respectively, and kept constant for all the simulations.

The SW, as defined by Eq. (3), takes into account all the components of the stress and of the strain rate tensor, without differentiating between extensional and shear components. Stadlbauer *et al.* (2004) performed a study on the effect of mechanical work in enhancing the nucleation density for an under-cooled polypropylene melt and suggested that there is not much difference between the influence of mechanical work put into the sample by shear flow or by extensional flow. However, extension could be more effective than shear in inducing FIC [see, for example, recent work by Hadinata *et al.* (2007)] and, in order to obtain more accurate predictions, Eq. (3) might have to be modified introducing an appropriate weighting factor for the SW done in extensional regions of the flow. These regions could be identified, for instance, by applying the flow classification criterion proposed by Astarita (1979), which involves the calculation of the local rate of rotation with respect to the direction of stretch.

III. RESULTS AND DISCUSSION

A. FIB

Melt flow birefringence experiments were matched with numerical simulations over a range of conditions to verify that the simulations could accurately predict the local stress

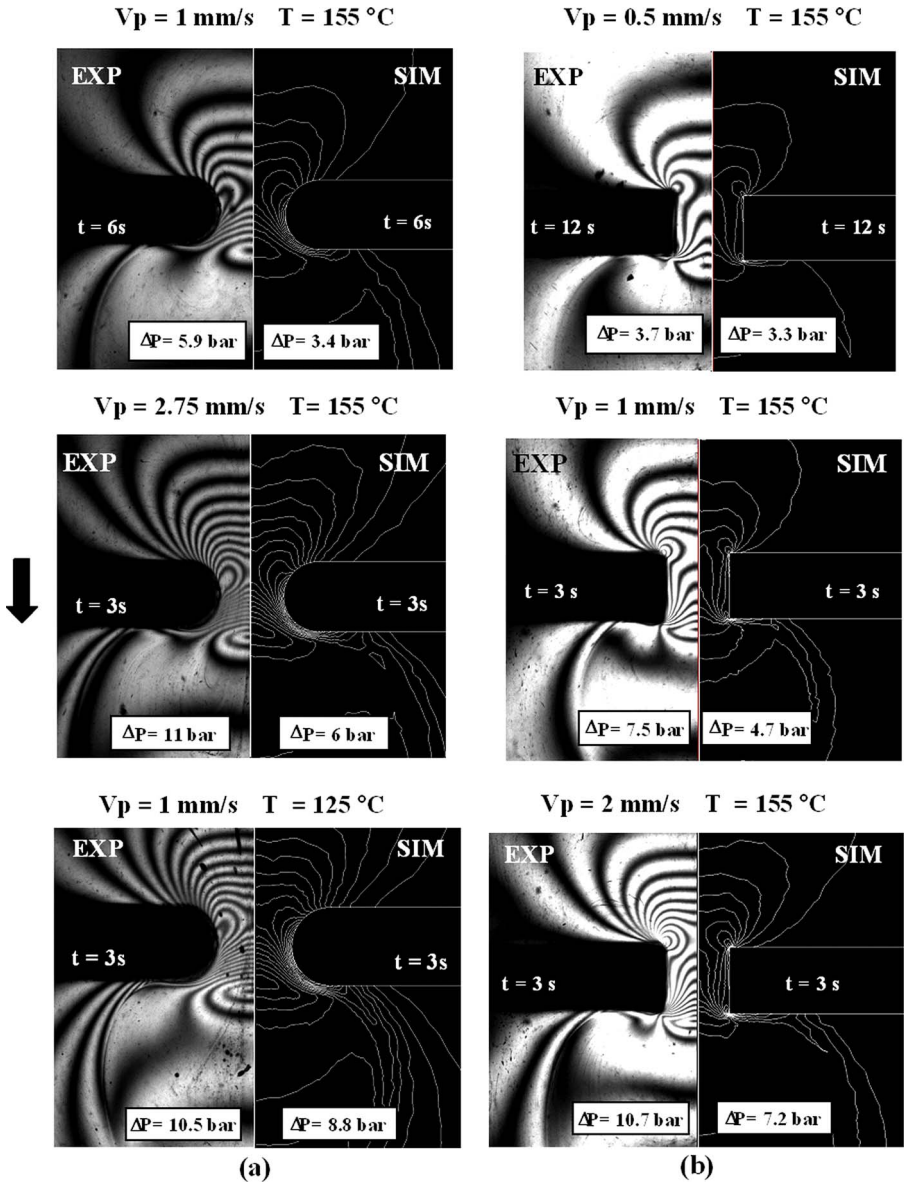

FIG. 3. Steady state matching of melt flow birefringence for DOW HDB6 flowing downward in a (a) CE-3 and (b) CE-1 geometry with FLOWSOLVE numerical simulations. Experimental fringe distribution and pressure difference for a range of conditions shown on the left hand side. Corresponding contours of calculated PSD and calculated pressure difference on the right hand side. The stress optical coefficient was equal to 18 $\times 10^{-9}$ Pa^{-1}.

in the flowing polymer when no crystallization occurred. Figure 3 shows some of the steady state matches for DOW HDB6 flowing downward for various piston speeds at 155 °C and 125 °C in both geometries. In view of the complexity of the flow field, the match between experiments and simulations was considered satisfactory for both the fringe distribution and the total pressure difference through the flow geometry.

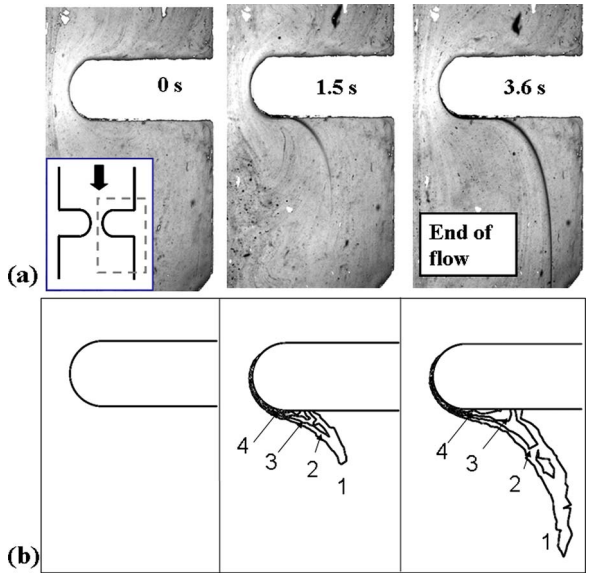

FIG. 4. DOW HDB6 in a rounded slit geometry at 125 °C and 2.75 mm/s piston speed ($\dot{\gamma}_{app,w} \approx 66\ s^{-1}$). Only half of the field of view is shown. (a) Sequence of images at different times after flow inception showing bright field observations in a region around one of the sidewalls and downstream. At $t=0$, before the pistons start moving downward, no crystals are present. At later times, a crystal filament (dark in the images) appears around the sidewalls and propagates downstream. The flow stops at $t=3.6$ s. (b) Contours of SW calculated by FLOWSOLVE. Each contour corresponds to a SW increment of 3 MPa. The region of localized FIC corresponds with the region of high SW.

B. FIC

1. Overview of the key experimental observations

Experimental observations of a HDPE melt flowing in an MPR optical cell and forming localized visible oriented crystals during flow were used to test the SW hypothesis. Isothermal flow experiments on HDB6 were performed at 125 °C (temperature for which the quiescent crystallization time scale is in the order of 2 h). These conditions were chosen to have a satisfactory visualization of FIC during flow under isothermal conditions. The cooling from high temperature took approximately 20 min, but the melt still appeared completely transparent before the inception of flow. Although some submicron nuclei were possibly present, it was assumed that no quiescent crystallization had occurred. Under the experimental conditions, flow can induce FIC in less than a second, so quiescent crystallization during the flow time (a few seconds) was negligible and all the crystals formed were those induced by flow. The heterogeneous nucleation from impurities present in the polymer at the start of the experiment was equally negligible. After isothermal FIC, the temperature was kept constant for 20 min to prove the stability of the flow-induced crystals then the MPR was heated at approximately 3 °C/min to a final temperature of 170 °C to melt the crystals and erase the thermo-mechanical history. During heating, the flow-induced crystals were stable up to a certain temperature (in the order of 135 °C–150 °C) and then melted.

The key observation [Fig. 4(a)] is the formation of very narrow localized crystal filaments, originating near the sidewalls of the slit inserts and propagating downstream. The crystals start appearing in the very early stages following flow inception, grow during flow, and do not further evolve after flow cessation (on a time scale of approxi-

mately 30 min). Light scattering effects from the crystallized material appear to be stronger than any birefringence effect, and, if observed with crossed polarizers, the filaments do not appear as highly birefringent regions. However, proof of the crystalline nature of such filaments was given by Hassell and Mackley (2008), who generated similar filaments for the same material at 125 °C in an entry-exit slit and then reversed the flow and observed the filament folding back on itself like a flexible solid. Further evidence of crystallinity of these structures and of their orientation at the nanoscale can be found in Mackley *et al.* (2000) and Hernandez de Muller (2008), who performed combined rheo-optical and wide angle x-ray diffraction studies on a supercooled HDPE crystallizing in similar conditions. The diffraction patterns for the sheared material showed equatorial spots and an amorphous halo, revealing the presence of crystals highly oriented in the flow direction and surrounded by polymer that was still molten.

2. Overview of the distribution of the calculated SW

Images of the crystal evolution during the piston movement at different times were compared with maps of SW distribution in the flow field calculated by FLOWSOLVE. The correlation between the regions of localized FIC and the regions of high SW was immediately apparent. Figure 4(a) shows bright field images at different times during flow of HDB6 in a rounded slit (CE-3) and Fig. 4(b) shows the corresponding contour map of simulated SW in the flow field. The dark regions in the experimental images, corresponding to a region of oriented visible FIC, are in similar positions as the high SW region. The SW was calculated through melt flow numerical simulations, which do not take into account the presence of the crystals. In most of the domain, this approximation is justifiable by the fact that the small and localized crystals do not affect the global flow field. However, once a crystal filament has formed, its presence will affect the local flow field—notably in the region near the crystal tip—and will substantially alter the hydrodynamic forces dominating further crystal growth [Mackley *et al.* (1975)]. Moreover, the presence of the first crystals provides nucleation sites enhancing the development of further FIC. For this reason, rather than trying to match at any time the regions of FIC with the regions of high SW, the SW criterion was applied focusing exclusively on the onset of FIC, postulating that FIC occurs when the SW that has accumulated along an adequately chosen trajectory reaches a critical value.

Provided the stretch condition of Eq. (6) is locally satisfied, in channel flows with no slip boundary conditions the analytical value of the SW at the walls diverges to infinity [Eq. (2)] due to the infinite residence time of the fluid near the wall, where both stress and strain rate are nonzero. Figure 5 illustrates the evolution of the numerically calculated SW as a function of the distance from the wall for HDB6 in a CE-3 geometry after 1.9 s from flow inception. The graph, which has a general validity, shows that the SW increases sharply as the distance from the wall decreases. FLOWSOLVE allows plotting the instantaneous streamlines of the flow field and, in light of the above consideration, the SW along a representative streamline has been monitored, in order to associate the maximum value of the SW accumulated along that streamline with the onset of FIC. During all the experiments performed, the crystal filaments appear only in a region very close to the wall. Ideally, the streamline chosen for the SW calculation should correspond to the position of the boundary between the crystal and the melt, so that the maximum of the SW on that streamline represents the critical SW for the onset of visible oriented FIC. In practice, this boundary is not easily resolvable, but from an analysis of the images, the width of the crystal filament appears to be in the order of 30–50 μm. Therefore, a

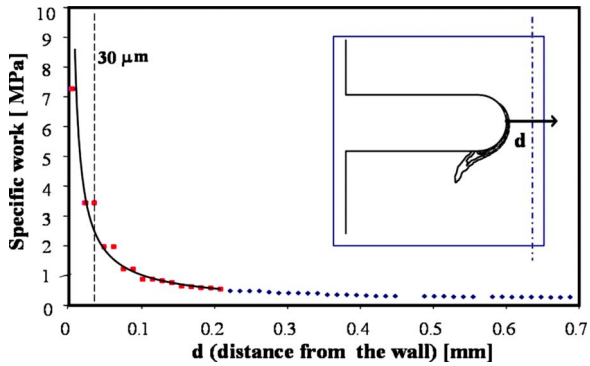

FIG. 5. Typical variation of the SW in CE-1 geometry along an horizontal cut at $Y=0$. The figure refers to a particular time and piston speed (respectively, 1.9 s and 1 mm/s), but has a more general value. SW increment between contours equal to 1.5 MPa

streamline has been chosen at 30 μm from the wall (at $y=0$) and called conventionally streamline α.

Starting from an initial time, each fluid element keeps accumulating SW as it flows along a given trajectory until the flow stops. The vertical velocity and—consequently—the residence time of the fluid in the midsection is highly dependent on the position of the trajectory. The fluid along the centerline flows with a maximum vertical velocity, whereas on trajectories near the wall the velocity is very low (due to the no slip boundary condition). Therefore, fluid elements flowing near the sidewalls accumulate work very slowly and the accumulated work has not reached a steady state when the flow stops (see Fig. 6). These considerations explain why the SW reaches a maximum (easily identifiable from the contour maps of SW distribution) near the exit of the contraction region and then

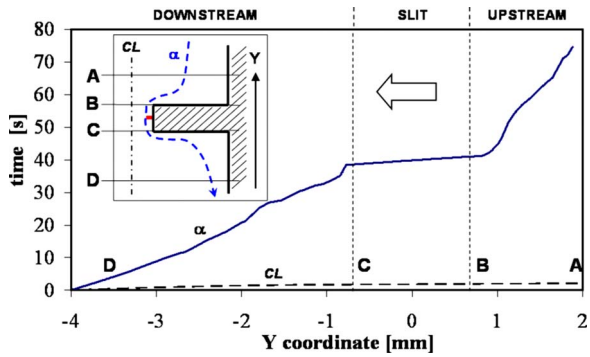

FIG. 6. Time needed by a fluid element to travel down along streamline α (full line) compared to the time needed to travel down the centerline (dashed line). Y is the axial coordinate, defined as zero in the middle of the contraction. The times to reach point D (at $Y=-4$) are shown as a function of the starting axial coordinate. Streamline α is defined as having a distance of 30 μm from the wall at $Y=0$. The figure refers to a simulation of melt flow of DOW HDB6 in geometry CE-1 at 125 °C and 1 mm/s piston speed at time of 11.46 s after flow inception. Along α, the residence time through the contraction region (B to C) is about 2.6 s, whereas it takes much higher time for the fluid to travel downward once it has reached the downstream region. This is mainly due to the fluid slowing down due to increased cross sectional area. The total time for a fluid element to travel through the whole observation field (from A to D) is in the order of 75 s. The cumulative SW along streamline α would need 75 s to reach the steady state in the whole domain. On the other hand, the fluid at the centerline travels from A to D in only 2 s.

decreases, instead of continuously accumulating along the streamlines in the downstream region. Fluid elements on streamline α, which—at the current time—are considerably downstream of the slit exit, have accumulated very little SW because at $t=0$ s (corresponding to flow inception), they started their journey from a position already downstream of the contraction region.

3. Results and discussion

A series of isothermal experiments on HDB6 at 125 °C flowing in a CE-1 and in a CE-3 geometry were performed for a range of piston speeds. Those are essentially 2D contraction-expansion slits; CE-1 has sharp corners, CE-3 completely rounded. Refer to Fig. 1 for schematics and dimensions. Although the two slits have the same width in their narrowest part, a considerable difference was observed between the FIC behaviors of the polymer in the two geometries. In the case of CE-1 (sharp), piston speeds as low as 1 mm/s were able to induce the formation of a crystal filament, whereas the onset of FIC using CE-3 (rounded) was observed for a piston speed of 2 mm/s. Numerical simulations were performed to investigate the amount of SW that the polymer undergoes in each flow field and to identify the value of critical SW for the onset of visible FIC of HDB6 at 125 °C.

Figures 7 and 8 show the development of FIC for HDB6 flowing downward at 125 °C and several piston speeds in CE-3 and CE-1 geometries, respectively. Sequences of bright field images captured at different times during flow until flow cessation allowed the determination of the piston speed at which visible FIC started occurring. The images show only one-half of the field of view, which is symmetrical, and the slit inserts are shown in white with dark borders to allow easier identification of the region of crystal formation. For the CE-3 geometry at 1 mm/s, no flow induced crystallization occurs [Fig. 7(a)] and a piston speed of 2 mm/s has been identified as the lowest piston speed able to generate a flow-induced crystal filament, barely visible as a dark line near the side walls and in the downstream fang region [Fig. 7(b)]. At 2.75 mm/s FIC is clearly present and at 10 mm/s even more FIC occurs, although it is still very localized [Figs. 7(c) and 7(d)]. Analogous considerations hold for FIC in the CE-1 geometry, although in this case the point of incipient FIC is at 1 mm/s (Fig. 8). Although the boundary between the lack of visible FIC and the onset of visible FIC is not very well defined, it has been shown that the sharp cornered slit can induce FIC more easily than a rounded slit. In all the experiments, the stroke amplitude was 10 mm and no further FIC occurred after flow cessation on a time scale of 30 min.

Numerical simulations were performed to better understand this experimental trend. Using the approach outlined in an earlier paragraph, the SW undergone by the fluid on streamline α was monitored as a function of the time elapsed from the moment of flow inception. In all cases, the transient SW was monitored up to times that were higher than the time at which flow-induced crystals started appearing (or until stroke completion in case no FIC was observed). The SW accumulates throughout the contraction region and reaches a maximum shortly after the slit exit. Figures 9 and 10 show the SW distribution along streamline α for the two geometries at 1 mm/s piston speed. The maximum value of the SW reaches its steady state value after the first 2 s. From 2 to 10 s, there is a considerable evolution of the SW only downstream of the slit exit. In the rounded geometry (CE-3) the SW starts gradually accumulating in the contraction region, reaches a maximum, and then smoothly decreases. The maximum shifts downstream as the stress field develops (Fig. 9). In the sharp cornered geometry (CE-1) similar trends are observed, but a peak in the SW was observed near the exit corner (Fig. 10). Due to

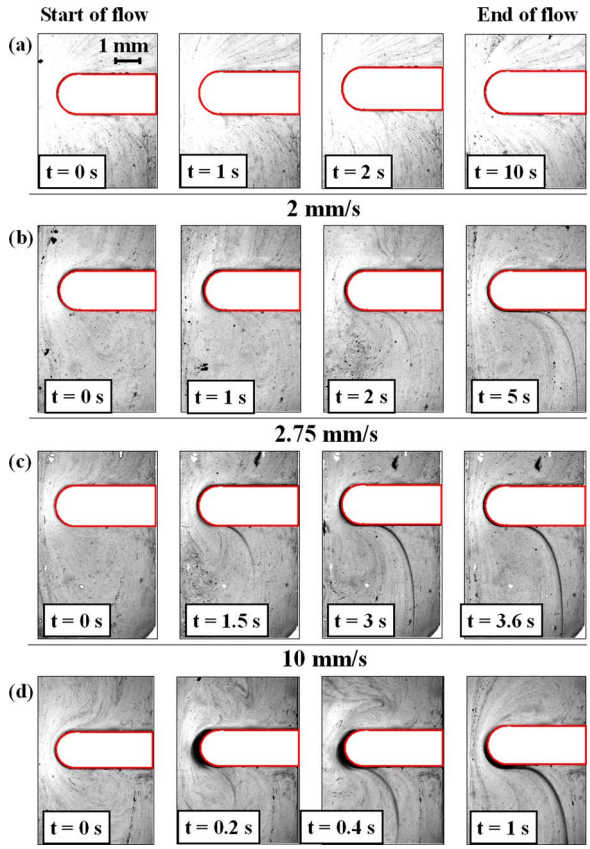

FIG. 7. Bright field observation of DOW HDB6 flowing downward at 125 °C in a CE-3 geometry. Only half of the field of view is shown. Images at different times after flow inception for different piston speeds. (a) 1 mm/s—no FIC is observed, (b) 2 mm/s—onset of visible FIC, (c) 2.75 mm/s—visible FIC occurs; (d) 10 mm/s—more FIC occurs, but the crystals are still localized. The last image of each set corresponds to the time of flow cessation. No further rapid crystal development was observed after that time.

numerical noise in the calculated SW, the curves were smoothed using a 20-point moving average trend line. The left hand side of Fig. 11 reports the time evolution of the maximum value of transient SW along streamline α in the two geometries for different piston speeds until the cessation of flow. The maximum of SW starts from zero and then builds up over time and saturates to a steady state value. The numerical curves of SW were compared to experimental observation of FIC. The right hand side of Fig. 11 shows bright field MPR observations at the end of the piston movement for experimental conditions corresponding to those of the SW calculations. Curve (a) corresponds to observations of no visible FIC, whereas curve (d) can be associated with the formation of a well-defined crystal filament. Curves (b) and (c) can be related to the incipient formation of a crystal filament, respectively, for the CE-3 and CE-1 geometry, and in the corresponding images the crystals are barely visible. The value of the critical SW for the onset of visible oriented FIC for HDB6 at 125 °C according to our criterion was determined to be in the range 9–11 MPa. Although expected to be very dependent on the material and the temperature, the value obtained is comparable to values reported by Mykhaylyk *et al.* (2008) for FIC of different grades of polyolefins. The application of a SW criterion appears to be

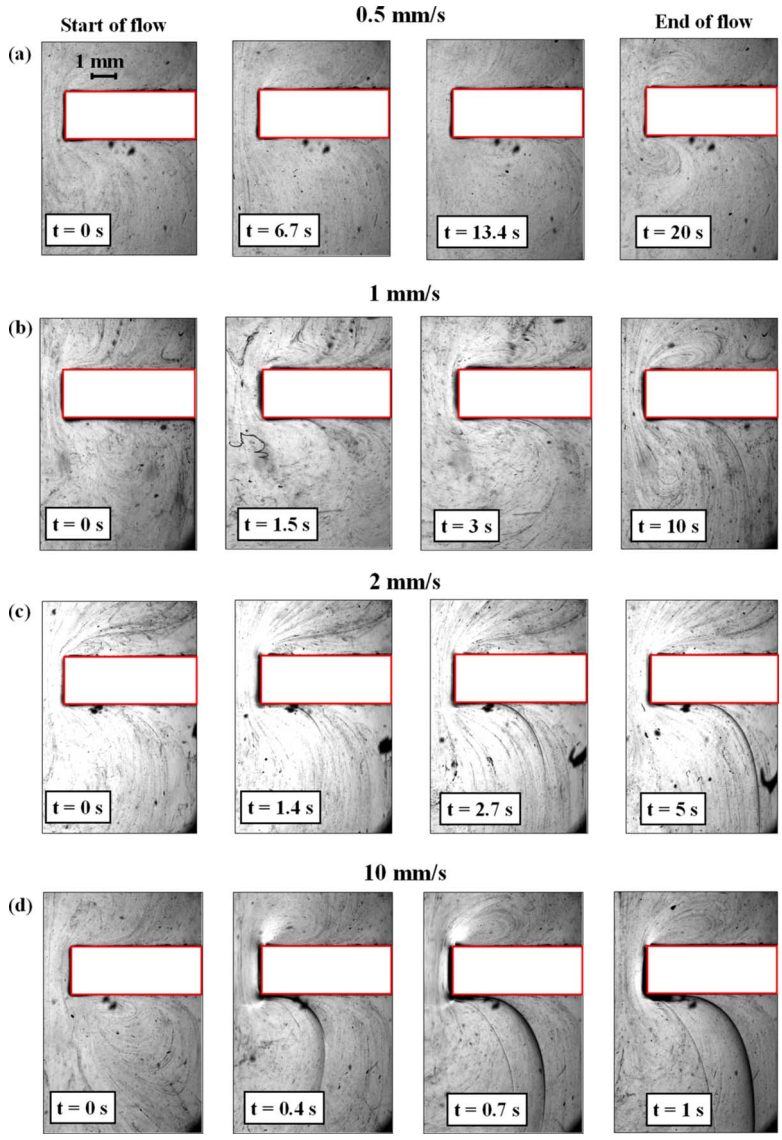

FIG. 8. Bright field observation of DOW HDB6 flowing downward at 125 °C in a CE-1 geometry. Only half of the field of view is shown. Images at different times after flow inception for different piston speeds. (a) 0.5 mm/s—no FIC is observed, (b) 1 mm/s—onset of visible FIC, (c) 2 mm/s—visible FIC occurs; (d) 10 mm/s—more FIC occurs, but the crystals are still localized. The last image of each set corresponds to the time of flow cessation. No further rapid crystal development was observed after that time.

consistent with the experimental observations reported in this paper and the concept of SW has the potential to be successfully applied to model FIC in complex flow processing conditions.

IV. CONCLUSIONS

Experimental observations of a HDPE crystallizing during flow in two different entry-exit optical cells were matched with viscoelastic numerical simulations. FLOWSOLVE

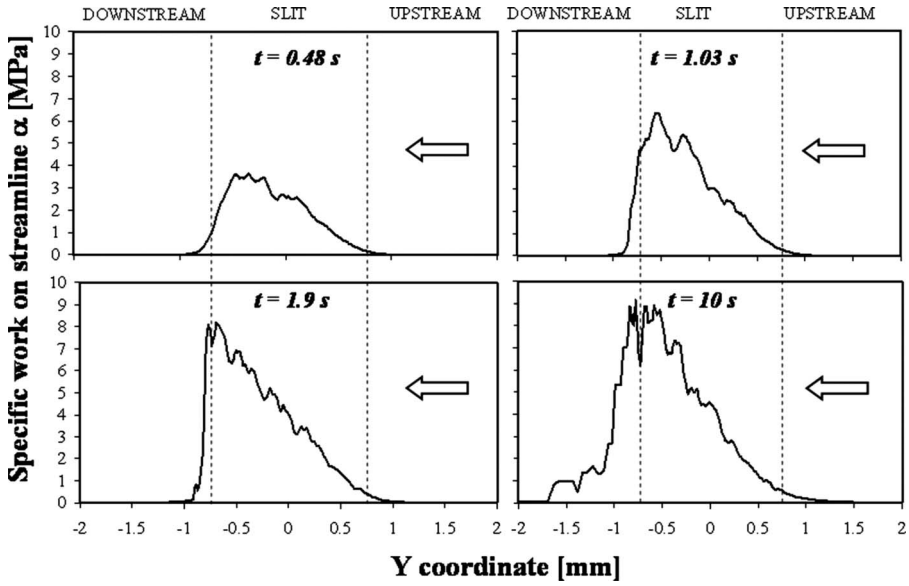

FIG. 9. Distribution of the SW along streamline α for different times after flow inception in a CE-3 geometry. Data shown for a piston speed of 1 mm/s. The SW gradually builds up in as the fluid travels through the rounded contraction and reaches its maximum just downstream of the slit exit. The same SW distribution can be observed at other piston speeds. All numerical data curves smoothed using 20-point moving average trend lines.

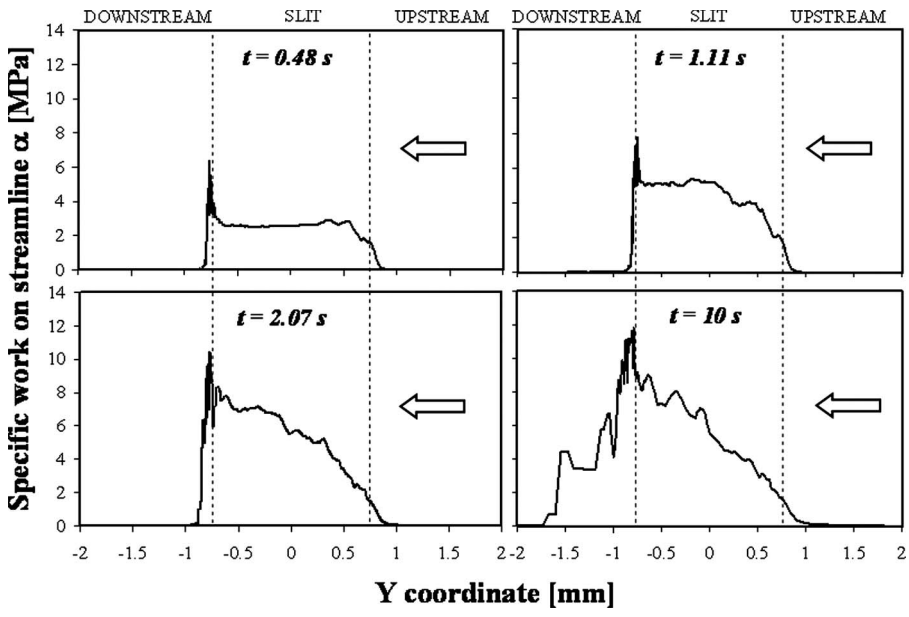

FIG. 10. Distribution of the SW along streamline α for different times after flow inception in a CE-1 geometry. Data shown for a piston speed of 1 mm/s. The SW reaches a peak just downstream of the slit exit. The same SW distribution can be observed at other piston speeds. From 2 to 10 s, there is a considerable evolution of the SW only downstream of the slit exit. All numerical data curves have been smoothed using 20 point-moving average trend lines.

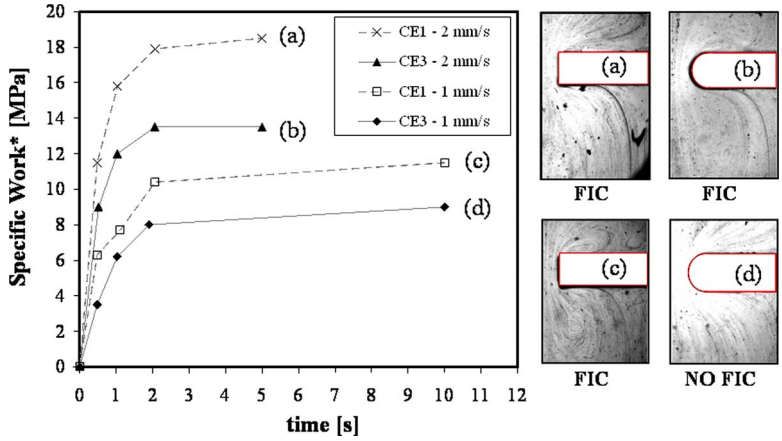

FIG. 11. Transient evolution of the maximum value of the SW accumulated along the instantaneous streamline α (indicated as specific work*) and its relation with the onset of FIC. The curves refer to both CE-1 and CE-3 geometries at both 1 mm/s and 2 mm/s piston speed. In the case of CE-3, the SW accumulated is lower than in CE-1. Experimentally, FIC is observed in all cases except for CE-3 at 1 mm/s, which corresponds to the lowest of the curves. It was then possible to identify the value of critical SW which causes the onset of visible FIC. The critical SW is in the range 9–11 MPa.

simulations using an 11-mode Pom-Pom model were then compared to melt flow birefringence observations for a range of conditions and gave good agreement in both the steady state principal stress difference (PSD) distribution and overall pressure drop.

Subsequently, an algorithm to calculate the local SW undergone during flow by the polymer fluid was implemented in the numerical code to investigate the relation between SW and local regions of FIC. Under the experimental conditions, the key observation was the formation during flow of narrow localized crystal filaments, originating near the sidewalls of the slit and propagating downstream in the "fang" region. A series of isothermal experiments were performed for a range of flow conditions and the piston speed corresponding to the onset of visible FIC was identified for each geometry. Numerical simulations were then performed to investigate the amount of SW that the polymer undergoes in each case to determine the value of critical SW for the onset of visible FIC for a specific HDPE melt (DOW HDB6) at 125 °C.

The match between experiments and SW simulations revealed that the regions of localized FIC corresponded to the regions of high SW. A method to obtain a quantitative relationship between the SW and FIC was proposed, postulating that FIC starts occurring when transient SW accumulated along a given fluid trajectory exceeds a critical value. The value of critical SW obtained—although expected to be very material and temperature specific—was consistent with the values obtained for another polyethylene melt under different experimental conditions by Mykhaylyk *et al.* (2008). This paper provides an example of implementation of the SW criterion in transient and complex ("processing-like") flows and shows the SW predictions to be consistent with experimental observations. In particular, the SW can be used to identify the onset of localized FIC. The outlined approach constitutes a platform upon which more detailed studies involving different geometries can be performed.

ACKNOWLEDGMENTS

The authors would like to acknowledge Dr. Dietmar Auhl for the linear and non-linear rheology. We also acknowledge the EPSRC for funding through the μPP^2 program (Microscale Polymer Processing 2) and Dow Benelux for providing the material.

References

Astarita, G., "Objective and generally applicable criteria for flow classification," J. Non-Newtonian Fluid Mech. **6**, 69–76 (1979).

Avrami, M., "Kinetics of phase change," J. Chem. Phys. **7**, 1103–1112 (1939).

Baaijens, F. P. T., "Mixed finite element methods for viscoelastic flow analysis: A review," J. Non-Newtonian Fluid Mech. **79**(2-3), 361–385 (1998).

Balzano, L., N. Kukalyekar, S. Rastogi, G. W. M. Peters, and J. C. Chadwick, "Crystallization and dissolution of flow-induced precursors," Phys. Rev. Lett. **100**, 048302 (2008).

Billon, N., V. Henaff, E. Pelous, and J. M. Haudin, "Transcrystallinity effects in high-density polyethylene. I. Experimental observations in differential scanning calorimetry analysis," J. Appl. Polym. Sci. **86**, 725–733 (2002).

Collis, M. W., and M. R. Mackley, "The melt processing of monodisperse and polydisperse polystyrene melts within a slit entry and exit flow," J. Non-Newtonian Fluid Mech. **128**, 29–41 (2005).

Doufas, A. K., I. S. Dairanieh, and A. J. McHugh, "A continuum model for flow-induced crystallization of polymer melts," J. Rheol. **43**(1), 85–109 (1999).

Eder, G., H. Janeschitz-Kriegl, and S. Liedauer, "Crystallization processes in quiescent and moving polymer melts under heat transfer conditions," Prog. Polym. Sci. **15**(4), 629–714 (1990).

Hadinata, C., D. Boos, C. Gabriel, E. Wassner, M. Rüllmann, N. Kao, and M. Laun, "Elongation-induced crystallization of a high molecular weight isotactic polybutene-1 melt compared to shear-induced crystallization," J. Rheol. **51**(2), 195–215 (2007).

Harlen, O. G., J. M. Rallison, and P. Szabo, "A split Lagrangian–Eulerian method for simulating transient viscoelastic flows," J. Non-Newtonian Fluid Mech. **60**, 81–104 (1995).

Hassell, D. G., and M. R. Mackley, "Localised flow-induced crystallisation of a polyethylene melt," Rheol. Acta **47**(4), 435–446 (2008).

Heeley, E. L., C. M. Fernyhough, R. S. Graham, P. D. Olmsted, N. J. Inkson, J. Embery, D. J. Groves, T. C. B. McLeish, A. C. Morgovan, F. Meneau, W. Bras, and A. J. Ryan, "Shear-induced crystallization in blends of model linear and long chain branched hydrogenated polybutadienes," Macromolecules **39**(15), 5058–5071 (2006).

Hernandez de Muller, G., "The effect of flow on the crystallisation of polyethylene," Ph.D. thesis, University of Cambridge, 2008.

Housmans, J. W., "Flow-induced crystallization of isotactic polypropylenes," Ph.D. thesis, TU Eindhoven, 2008.

Janeschitz-Kriegl, H., E. Ratajski, and M. Stadlbauer, "Flow as an effective promotor of nucleation in polymer melts: A quantitative evaluation," Rheol. Acta **42**, 355–364 (2003).

Jay, F., J. M. Haudin, and B. Monasse, "Shear-induced crystallization of polypropylenes: Effect of molecular weight," J. Mater. Sci. **34**(9), 2089–2102 (1999).

Jerschow, P., and H. Janeschitz-Kriegl, "On the development of oblong particles as precursors for polymer crystallization from shear flow: Origin of the so-called fine grained layers," Rheol. Acta **35**(2), 127–133 (1996).

Keller, A., "Polymer crystals," Rep. Prog. Phys. **31**, 623–704 (1968).

Keum, J. K., F. Zuo, and B. S. Hsiao, "Formation and stability of shear-induced shish-kebab structure in highly entangled melts of UHMWPE/HDPE blends," Macromolecules **41**(13), 4766–4776 (2008).

Kumaraswamy, G., R. K. Verma, A. M. Issaian, P. Wang, J. A. Kornfield, F. Yeh, B. S. Hsiao, and R. H. Olley, "Shear-enhanced crystallization in isotactic polypropylene Part 2. Analysis of the formation of the oriented skin," Polymer **41**(25), 8931–8940 (2000).

Kumaraswamy, G., J. A. Kornfield, F. Yeh, and B. S. Hsiao, "Shear-enhanced crystallization in isotactic polypropylene. 3. Evidence for a kinetic pathway to nucleation," Macromolecules **35**(5), 1762–1769 (2002).

Kumaraswamy, G., J. A. Kornfield, F. Yeh, and B. S. Hsiao, "Shear-enhanced crystallization in isotactic polypropylene. In-situ synchrotron SAXS and WAXD," Macromolecules **37**(24), 9005–9017 (2004).

Liedauer, S., G. Eder, H. Janeschitz-Kriegl, P. Jerschow, W. Geymayer, and E. Ingolic, "On the kinetics of shear

induced crystallization in polypropylene," Int. Polym. Process. **8**, 236–244 (1993).

Mackley, M. R., and A. Keller, "Flow-induced crystallization of polyethylene melts," Polymer **14**, 16–20 (1973).

Mackley, M. R., F. C. Frank, and A. Keller, *Flow-Induced Crystallization of Polyethylene Melts* (Journal of Materials Science-Springer, New York, 1975).

Mackley, M. R., O. Saquet, and G. Moggridge, "Direct experimental evidence for flow induced fibrous polymer crystallisation occurring at a solid/melt interface," J. Mater. Sci. **35**, 5247–5253 (2000).

Matsuba, G., S. Sakamoto, Y. Ogino, K. Nishida, and T. Kanaya, "Crystallization of polyethylene blends under shear flow. Effects of crystallization temperature and ultrahigh molecular weight component," Macromolecules **40**(20), 7270–7275 (2007).

McHugh, A. J., D. A. Tree, B. Pornimit, and G. W. Ehrenstein, "Flow-induced crystallization and self-reinforcement during extrusion," Int. Polym. Process. **VI**, 208–211 (1991).

McLeish, T. C. B., and R. C. Larson, "Molecular constitutive equations for a class of branched polymers: The Pom-Pom polymer," J. Rheol. **42**(1), 81–110 (1998).

Mykhaylyk, O., P. Chambon, R. S. Graham, P. A. Fairclough, P. D. Olmsted, and A. J. Ryan, "The specific work of flow as a criterion for orientation in polymer crystallization," Macromolecules **41**(6), 1901–1904 (2008).

Nicholson, T. M., *FlowSolve: A Lagrangian Flow Solver for Complex Flows in Polymers—Developers Manual* (University of Leeds, UK, 2000).

Peters, G. M. W., "A computational model for processing of semi-crystalline polymers: The effects of flow-induced crystallization," Lect. Notes Phys. **606**, 312–324 (2003).

Scelsi, L., and M.R. Mackley, "Rheo-optic flow-induced crystallisation of polypropylene and polyethylene within confined entry-exit flow geometries," Rheol. Acta **47**(8), 895–908/1435–1528 (2008).

Seki, M., D. W. Thurman, J. P. Oberhauser, and J. A. Kornfield, "Shear-mediated crystallization of isotactic polypropylene: The role of long chain-long Chain overlap," Macromolecules **35**(7), 2583–2594 (2002).

Smirnova, J., L. Silva, B. Monasse, J. Chenot, and J. Haudin, "Structure development in injection molding," Int. Polym. Process. **20**(2), 178–185 (2005).

Somani, R. H., L. Yang, L. Zhu, and B. S. Hsiao, "Flow-induced shish-kebab precursor structures in entangled polymer melts," Polymer **46**(20), 8587–8623 (2005).

Stadlbauer, M., H. Janeschitz-Kriegl, G. Eder, and E. Ratajski, "New extensional rheometer for creep flow at high tensile stress. Part II. Flow induced nucleation for the crystallization of iPP," J. Rheol. **48**(3), 631–639 (2004).

Van Puyvelde, P., F. Langouche, and J. Baert, "Flow-induced crystallization in poly-1-butene: The shish-kebab transition," Int. J. Mat. Form. **1**, (S1), 667–670 (2008).

Woods-Adams, P., and S. Costeux, "Thermorheological behaviour of polyethylene: Effects of microstructure and long chain branching," Macromolecules **34**, 6281–6290 (2001).

Zuidema, H., G. W. M. Peters, and H. E. H. Meijer, "Development and validation of a recoverable strain-based model for flow-induced crystallization of polymers," Macromol. Theory Simul. **10**, 447–460 (2001).